ChemComm

COMMUNICATION

View Article Online
View Journal | View Issue

Cite this: *Chem. Commun.*, 2019, 55, 818

Received 7th August 2018,
Accepted 12th December 2018

DOI: 10.1039/c8cc06410e

rsc.li/chemcomm

Formation of unexpectedly active Ni–Fe oxygen evolution electrocatalysts by physically mixing Ni and Fe oxyhydroxides†

Mikaela Görlin, *[abc] Petko Chernev,[a] Paul Paciok,[d] Cheuk-Wai Tai,[e] Jorge Ferreira de Araújo,[b] Tobias Reier,[b] Marc Heggen,[d] Rafal Dunin-Borkowski,[d] Peter Strasser[b] and Holger Dau[a]

We present an unusual, yet facile, strategy towards formation of physically mixed Ni–Fe(O_xH_y) oxygen evolution electrocatalysts. We use *in situ* X-ray absorption and UV-vis spectroscopy, and high-resolution imaging to demonstrate that physical contact between two inferior $Ni(OH)_2$ and Fe(OOH) catalysts self-assemble into atomically intermixed Ni–Fe catalysts with unexpectedly high activity.

The emerging global energy challenge requires development of renewable energy technologies.[1–3] One way to harvest energy is to oxidize substrate water using photovoltaic and electrolyzer devices,[4–6] which allow further conversion into H_2 or higher carbon fuels using the released electrons and protons in electroreduction processes.[7,8] The oxygen evolution reaction (OER) is the most demanding electrochemical half-cell reaction in water splitting, predicted to proceed *via* coupled four proton–electron transfer steps involving scaling relations between surface adsorbed intermediates (OH*, O*, OOH*).[9] While Ru and Ir oxides are preferred catalysts in acidic media,[10,11] non-noble metal oxides show outstanding activities under near neutral[12] to alkaline conditions,[13–15] where the state-of-the-art catalyst is currently bimetallic combinations of Ni–Fe.[16–19] Boettcher and co-workers presented evidence using XPS in combination with a new purification method, that Fe impurities from the electrolyte are readily incorporated into the $Ni(OH)_2$ lattice.[18] Investigations using X-ray absorption spectroscopy (XAS) have provided further insight into the active site of Ni–Fe catalysts. The metal redox states are however subjected to debate. The metals reside as Ni^{2+} and Fe^{3+} at resting potential. During OER, the Ni-site is oxidized from Ni^{2+} to $Ni^{3+/4+}$, whereas Fe has mostly been observed to partly change population towards low-valent Ni^{2+};[20–25] however, it has also been seen to promote Ni^{4+}.[26] Fe usually passivates (Fe^{3+});[20,23,24,27] however, some studies have observed oxidized Fe^{4+}[28–30] and Fe^{6+}.[31] The first DFT+U study by Friebel *et al.*[27] presented evidence that Fe is the active site due to optimal overpotential. Ahn *et al.*[32] observed the presence of "fast" and "slow" sites in the Ni–Fe catalysts using scanning electrochemical microscopy – where the fast sites matched the Fe-content. A recent computational study by Goddard and coworkers instead showed that O–O coupling is more likely to occur at Ni-sites; however, it requires the synergy from the mixed Ni–Fe site.[25] Burke Stevens *et al.*[33] reported the formation of Ni–O–Fe sites at the "surface" of NiOOH upon cycling in an electrolyte intentionally spiked with Fe^{3+}, and proposed that surface sites are more reactive than bulk sites. Similar studies showing formation of bimetallic Ni–Fe catalysts were presented by Yin *et al.*[34] using Ni-foam and by Wang *et al.*[35] using NiOOH, also in the Fe^{3+} spiked electrolyte.

In this contribution, we provide new insights on a facile preparation procedure of Ni–Fe catalysts, formed by "physically mixing" two chemically distinct $Ni(OH)_2$ and Fe(OOH) materials, with an unexpectedly high OER activity. We provide detailed electrochemical, spectroscopic and microscopic investigations (XAS, UV–vis, HAADF-STEM, and EDX elemental mapping) to pin down the origin of the catalytic site.

The parental $Ni(OH)_2$ and FeOOH oxide catalysts were synthesized according to a reported solvothermal method.[20] Two ink formulations of the individual parental oxides were mixed by brief sonication (see ESI† for details). Scanning electron microscopy (SEM) confirmed that both $Ni(OH)_2$ and Fe(OOH) were particle-like in the size range of ~200–500 nm, whereas the $Ni_{100}(OH)_2$ catalyst was composed of typical randomly stacked hydroxide sheets (Fig. S1a and b, ESI†).[36,37] The physical mixture ("p.m.") appeared as a composite of the two, and the SEM-EDX elemental mappings indicated that Ni and Fe were more or less well distributed (Fig. S1c and d, ESI†). The local mixing will be further investigated below. The activities were

[a] *Department of Physics, Free University of Berlin, 14195 Berlin, Germany*
[b] *The Electrochemical Energy, Catalysis, and Materials Science Laboratory, Department of Chemistry, Technical University of Berlin, 10623 Berlin, Germany*
[c] *Department of Physics, AlbaNova University Centre, Stockholm University, SE-10691 Stockholm, Sweden. E-mail: mikaela.gorlin@fysik.su.se*
[d] *Ernst Ruska-Centre for Microscopy and Spectroscopy with Electrons, Forschungszentrum Jülich, Jülich, Germany*
[e] *Department of Materials and Environmental Chemistry, Stockholm University, SE-106 91, Sweden*

† Electronic supplementary information (ESI) available: Experimental details, electrochemical characterization, UV-vis, Faradaic efficiency calculations, and XAS simulations and fit parameters. See DOI: 10.1039/c8cc06410e

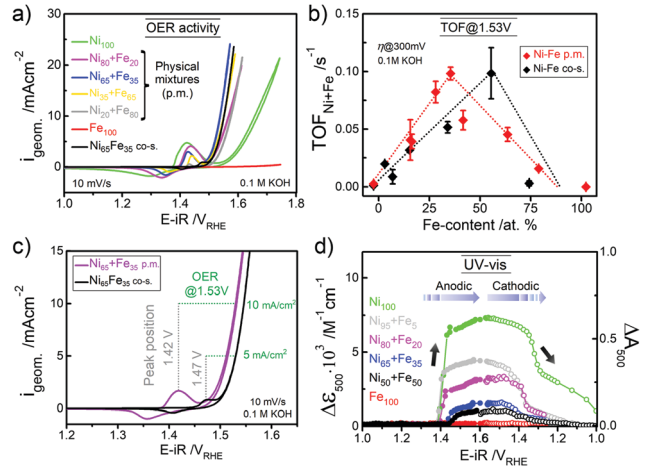

Fig. 1 (a) The OER activity (CVs at 10 mV s^{-1}) of physically mixed (p.m.) Ni + Fe catalysts and a co-synthesized (co-s.) Ni–Fe catalyst. (b) TOF_{Ni+Fe} per total metal ion at η = 300 mV at a total metal loading of ~25 μg_{Ni+Fe} cm^{-2}. (c) CVs of the Ni_{65} + Fe_{35} p.m. and co-s. $Ni_{65}Fe_{35}$ catalysts in as-received KOH. The position of the redox peaks and activity at 1.53 V is indicated with dotted lines. (d) *In situ* UV–vis absorption at λ = 500 nm (average between 400–600 nm) during potential staircase-wise steps. The physically mixed catalysts were measured in Fe-free KOH[18] and the Fe_{100}(OOH) catalyst in as-received KOH unless stated otherwise.

evaluated using a rotating disk electrode (RDE) setup (see details in ESI†). A composition-controlled activity was evident in our physically mixed catalysts, where in fact the activity of some of the Ni + Fe p.m. catalysts exceeded the activity of the co-s. catalysts (Fig. 1a). The turnover frequency per total metal ion (TOF_{Ni+Fe}) at η = 300 mV was highest around 30–35% Fe-content. Compared to the co-synthesized catalysts, the activity maximum was shifted to higher Ni-content in the physically mixed catalysts (Fig. 1b). The Ni_{65} + Fe_{35} p.m. catalyst had a highest turnover frequency of 0.1 s^{-1}, and exhibited an overpotential of 298 mV at 10 mA cm^{-2} and a Tafel slope of 37 mV dec^{-1} (Fig. S2a, b, eqn (S1)–(S2) and Table S1, ESI†). The faradaic efficiency (FE_{O_2}) was estimated to be 92% for a Ni_{50} + Fe_{50} p.m. catalyst (Fig. S2c, d and eqn (S3)–(S5), ESI†). We conclude that our physically mixed catalysts exhibit intrinsic turnover rates competitive to other Ni–Fe catalysts (see Table S2 for literature comparison, ESI†).[38] The only study known to us including physical mixtures of oxides was reported by Gong *et al.*,[16] wherein the resulting β-$Ni(OH)_2$NP + FeO_xNP in contrast showed inferior activity to the co-synthesized catalyst. This is surprising since several studies have shown that active Ni–Fe catalysts can be obtained by exposing Ni electrodes to an electrolyte containing Fe^{3+} impurities.[33–35,39] In our Ni + Fe catalysts, the Ni^{2+} → Ni^{3+} redox peaks were positioned at strikingly high cathodic potentials (by ~50 mV) compared to that of the co-s. Ni–Fe catalysts, and the integrated area (redox charge) was relatively higher (Fig. 1c and Fig. S3, ESI†). A similar difference in peak position was reported by Burke Stevens *et al.*[33] of an electrodeposited Ni(OOH) cycled in an Fe^{3+} spiked electrolyte and a co-deposited Ni–Fe catalyst, which was explained by a smaller number of Fe ions substituting "bulk" lattice sites. At a given nominal composition, it is hence likely that our Ni + Fe p.m. catalysts have an average lower number of mixed Ni–Fe sites. *In situ* UV-vis showed that the absorption perfectly matched the redox peaks in our Ni + Fe catalysts, which coincided with an increase in the absorption around ~500 nm assigned to the oxidized $Ni^{3+/4+}$ species (Fig. 1d and Fig. S4, S5, ESI†).[20] The Ni_{100} catalyst underwent a concomitant coloration from transparent to dark; however, increasing the Fe-content gradually prevented this color change in the Ni + Fe catalysts (Fig. S5a, ESI†), in agreement with our earlier studies of the co-s. Ni–Fe catalysts.[20] Total reflection X-ray fluorescence (TXRF) spectroscopy revealed a significant loss of Fe after the OER characterization protocol (see Fig. 2). Dissolution of Fe has been reported before in Ni–Fe catalysts; however, not to this extent.[40,41] Despite this, we noticed a steady increase in activity during the characterization along with an anodic peak shift (Fig. S6, ESI†). A less significant shift was seen for the $Ni_{100}(OH)_2$ catalyst, suggesting that Fe-impurities were not the main cause of this "activation". A similar activation was seen for the co-s. Ni–Fe catalysts, but less pronounced than for the Ni + Fe catalysts (Fig. S7, ESI†). This suggests that the activation may partly be due to other processes such as hydration in addition to possible compositional changes. The OER activities after correction for the dissolution of metals are shown in Fig. S2e (ESI†).

To better resolve the mixing and local atomic composition in the physically mixed catalysts, we used high-angle annular dark field imaging – scanning transmission electron microscopy (HAADF-STEM) and elemental mapping. Investigations of the as-prepared Ni_{50} + Fe_{50} p.m. catalyst showed that the parental $Ni(OH)_2$ and Fe(OOH) particles did not form a complete uniformly mixed phase (Fig. 3a, b and Fig. S8a–e, ESI†). EDX elemental mappings showed that only a small fraction of the particles formed a direct contact area (mixed Ni–Fe sites) and other areas were not in contact at all. The largest mixing occurred in the direct contact areas, and further away from this area Ni-rich and Fe-rich phases were clearly visible. In these half mixed $Ni(OH)_2$ and Fe(OOH) phases, there were about 1–2% of Fe and Ni impurities homogenously distributed over the entire particles, respectively. The mixing in the direct contact area is not well defined, and depends on the size and the thickness of the particles. After exposure to catalytic potential (1.63 V, 30 min in purified 0.1 M KOH), the impurities of both Ni and Fe increased in the respective phase

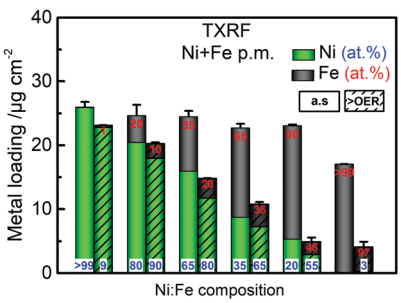

Fig. 2 TXRF analysis of p.m. Ni + Fe catalysts in 0.1 M KOH. Shown are the as-prepared (a.s) catalysts before the OER (left, solid bars) and after the OER characterization of ~2 h (right, hatched bars). Each bar is split into Ni content (green) and Fe content (black). The electrolyte was stripped of Fe-impurities, except for the Fe_{100}(OOH) catalyst.

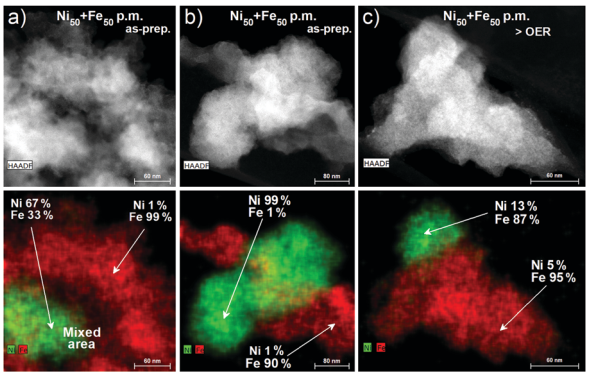

Fig. 3 The HAADF-STEM (upper panel) and EDX mapping overlays of Ni and Fe (lower panel) of a physically mixed (p.m.) Ni_{50} + Fe_{50} catalyst showing direct contact areas of mixed $Ni(OH)_2$ and Fe(OOH) particles (a) and (b) as-prepared Ni_{50} + Fe_{50} p.m. catalyst and (c) Ni_{50} + Fe_{50} p.m. after OER. Ni-rich areas are shown in green and Fe-rich in red. The samples were conditioned at 1.63 V for 30 min in Fe-free 0.1 M KOH.

segregated Ni-rich and Fe-rich areas of the Ni_{50} + Fe_{50} p.m. catalyst. The $Ni(OH)_2$ particles after OER contained ~4–13% of Fe impurities, and the Fe(OOH) particles ~4–8% of Ni impurities (Fig. 3c and Fig. S8f–j, ESI†). On average, the levels of impurities are in accordance with the limitation of ~25–30% solubility of Fe in the $Ni(OH)_2$/OOH phase.[27,33] We note that all catalyst particles had an oxide contribution of ~75%, which was present in both the Ni and Fe phases. Investigations of the as-prepared $Ni_{100}(OH)_2$ and Fe(OOH) materials showed that both contained a very low amount of impurities (<0.1%), see Fig. S9 (ESI†). Therefore, the elevated impurities in the mixed Ni + Fe catalysts are likely a result of the mixing. After OER, a small increase in Fe impurities in the $Ni_{100}(OH)_2$ catalyst was observed despite that the electrolyte had been purified (~1%), showing the difficulty to remove all sources of impurities. The more significant increase of impurities in the Ni_{50} + Fe_{50} p.m. catalyst during the OER may therefore be regarded to compositional changes, likely facilitated by the observed dissolution. For comparison, we investigated a co-synthesized $Ni_{40}Fe_{60}$ catalyst, which we confirmed was composed of a uniformly mixed Ni–Fe phase in contrast to the physically mixed catalyst (Fig. S10, ESI†). Our results therefore confirm that at any given nominal composition, the number of mixed Ni–Fe sites in our physically mixed Ni + Fe catalysts is smaller, and also smaller compared to the co-synthesized Ni–Fe catalysts at the actual composition. The intrinsic turnover rates in our Ni + Fe p.m. catalysts are therefore likely to be highly underestimated, assuming that a mixed Ni–Fe site is required for efficient catalysis, as proposed by Xio *et al.*[25] based on DFT calculations.

The local atomic structure was further investigated using *in situ* X-ray absorption spectroscopy (XAS) at the metal K-edges. The as-prepared Ni_{65} + Fe_{35} p.m. catalyst exhibited octahedral coordination with metal centers in Ni^{2+} and Fe^{3+} oxidation states, in agreement with the co-s. $Ni_{65}Fe_{35}$ catalyst and the parental $Ni(OH)_2$ and Fe(OOH) catalysts (Fig. 4 and Fig. S11, S12, ESI†).[20] The 2nd FT-EXAFS amplitude representing the Fe–M coordination shell of the as-prepared Ni_{65} + Fe_{35} p.m. catalyst was a bit higher than the parental Fe_{100}(OOH), which may indicate a small modulation of the Fe phase. The amplitudes were on the other hand lower than in the co-s. $Ni_{65}Fe_{35}$ catalyst showing that the bulk was not modified to the same extent, in agreement with the other data. Surprisingly, application of a catalytic potential of 1.63 V did not result in a Ni K-edge shift of the Ni_{65} + Fe_{35} p.m. catalyst, as expected for the $Ni^{2+} \rightarrow Ni^{3+/4+}$ oxidation. Therefore, all metal centers remained as low-valent Ni^{2+}. The parental $Ni_{100}(OH)_2$ on the other hand exhibited an edge shift of +2.6 eV as expected for "complete oxidation" to $Ni^{3.7+}$.[20] None of the investigated catalysts exhibited potential-induced changes at the Fe K-edge and therefore are compatible with Fe^{3+} throughout the reaction cycle.[20] This concludes that Fe sites in our Ni + Fe p.m. catalyst are more similar to the sites in the parental Fe_{100}(OOH) – in contrast to the Ni sites – which are more similar to the sites in the co-s. $Ni_{65}Fe_{35}$ catalyst. Operando XAS of a Ni_{50} + Fe_{50} p.m. catalyst also confirmed the absence of oxidation state changes, in accordance with the quasi-in situ XAS (Fig. S13, ESI†). It should be kept in mind that changes below ~10% may be difficult to observe since XAS is a bulk method. Simulated fit parameters are listed in Tables S3 and S4, ESI.†

It is somewhat unexpected that a relatively small amount of Fe contaminations in the $Ni(OH)_2$ phase is sufficient to suppress nearly the entire visible population of oxidized $Ni^{3+/4+}$. This is in agreement with our observations in the co-s. Ni–Fe catalysts that ~10% is sufficient to shift the equilibrium to the Ni^{2+} state during OER,[20] also supported by other studies.[22,23,25] An interesting similar effect of Fe was reported by Klaus *et al.*,[40] where a sputtered Fe top-layer on a sublayer of Ni inhibited the electrochemical conversion of metallic Ni to $Ni(OH)_2$/NiOOH, and hence Fe was proposed to act as a "capping" layer. It is therefore possible that the Fe(OOH) not incorporated into the $Ni(OH)_2$ phase may introduce similar unwanted effects.

To summarize, our XAS data is compatible with formation of new "interfacial" Ni–Fe sites in our physically mixed catalysts. This includes formation of a new atomically intermixed phase with bridging (physio-chemical) Ni–O–Fe motifs, which according to HAADF-STEM and mappings are restricted to some local spots

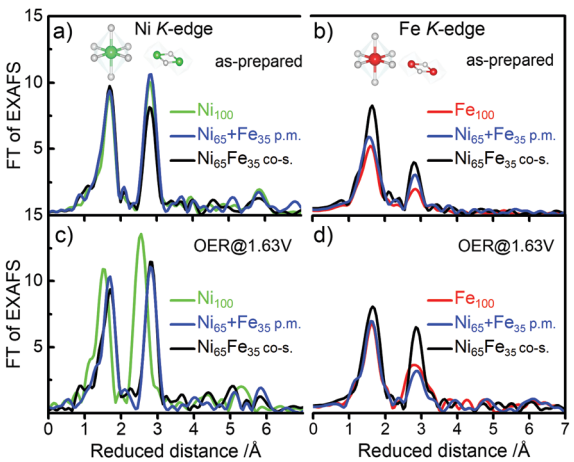

Fig. 4 (a) Ni K-edge k^3-weighted FT-EXAFS of pristine catalysts (before the OER) in the quasi-*in situ* setup at 20 K. (b) Fe K-edge of as-prepared catalysts. (c) Ni K-edge at 1.63 V. (d) Fe K edge at 1.63 V. The measurements were carried out in 0.1 M KOH.

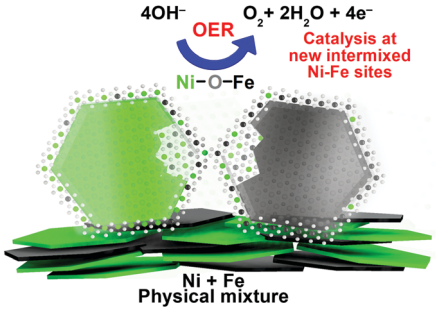

Fig. 5 Schematic active-site model in the physically mixed Ni + Fe(O_xH_y) OER electrocatalysts. The parental $Ni_{100}(OH)_2$ (green) and Fe(OOH) (black) mixes to form a "new" intermixed phase with Ni–(O)–Fe motifs, promoted in the direct contact area where highest mixing occurs. Some additional contaminations (~4–13%) are uniformly dispersed over the rest of the catalyst particles.

on the particles that form a direct contact area (depicted in Fig. 5). At a given composition, the number of mixed sites in the Ni + Fe p.m. catalysts is smaller in comparison to the co-synthesized catalysts. It is therefore remarkable that similar current densities are achieved with a different number of active sites. In recent discussions "surface", "edge" or "defect" sites were proposed as more reactive towards the OER than "bulk" sites.[30,33] In line with these discussions – the presence of two types of sites (or location) with distinct O_2 turnover rates would offer a feasible explanation for the unexpectedly high activity in our physically mixed Ni–Fe catalysts. We speculate whether these highly active sites are more "exposed" sites such as surface or edge sites.

We have shown that highly active OER catalysts can be prepared by facile mixing of distinct $Ni(OH)_2$ and Fe(OOH) phases, where a fraction self-assemble into mixed Ni–Fe sites, responsible for the activity.

We thank Helmholtz-Zentrum Berlin (HZB) for measurements at KMC-1 and KMC-3 at BESSY II (thanks Marcel Mertin, Ivo Zizak, Götz Schuck). We also thank Ulrich Gernert and Christoph Fahrenson at ZELMI Zentrum Berlin for SEM-EDX.

Conflicts of interest

There are no conflicts to declare.

Notes and references

1 N. S. Lewis and D. G. Nocera, *Proc. Natl. Acad. Sci. U. S. A.*, 2006, **103**, 15729–15735.
2 H. Dau, C. Limberg, T. Reier, M. Risch, S. Roggan and P. Strasser, *ChemCatChem*, 2010, **2**, 724–761.
3 D. Gust, T. A. Moore and A. L. Moore, *Acc. Chem. Res.*, 2009, **42**, 1890–1898.
4 J. Luo, J.-H. Im, M. T. Mayer, M. Schreier, M. K. Nazeeruddin, N.-G. Park, S. D. Tilley, H. J. Fan and M. Grätzel, *Science*, 2014, **345**, 1593–1596.
5 L. Wang, F. Dionigi, N. T. Nguyen, R. Kirchgeorg, M. Gliech, S. Grigorescu, P. Strasser and P. Schmuki, *Chem. Mater.*, 2015, **27**, 2360–2366.
6 S. Dresp, F. Luo, R. Schmack, S. Kuhl, M. Gliech and P. Strasser, *Energy Environ. Sci.*, 2016, **9**, 2020–2024.
7 C. W. Li and M. W. Kanan, *J. Am. Chem. Soc.*, 2012, **134**, 7231–7234.
8 H. Mistry, A. S. Varela, C. S. Bonifacio, I. Zegkinoglou, I. Sinev, Y.-W. Choi, K. Kisslinger, E. A. Stach, J. C. Yang, P. Strasser and B. R. Cuenya, *Nat. Commun.*, 2016, **7**, 12123.
9 I. C. Man, H. Y. Su, F. Calle-Vallejo, H. A. Hansen, J. I. Martinez, N. G. Inoglu, J. Kitchin, T. F. Jaramillo, J. K. Norskov and J. Rossmeisl, *ChemCatChem*, 2011, **3**, 1159–1165.
10 Y. Lee, J. Suntivich, K. J. May, E. E. Perry and Y. Shao-Horn, *J. Phys. Lett.*, 2012, **3**, 399–404.
11 T. Reier, H. N. Nong, D. Teschner, R. Schlögl and P. Strasser, *Adv. Energy Mater.*, 2017, **7**, 1601275.
12 M. Risch, F. Ringleb, M. Kohlhoff, P. Bogdanoff, P. Chernev, I. Zaharieva and H. Dau, *Energy Environ. Sci.*, 2015, **8**, 661–674.
13 C. C. L. McCrory, S. Jung, I. M. Ferrer, S. M. Chatman, J. C. Peters and T. F. Jaramillo, *J. Am. Chem. Soc.*, 2015, **137**, 4347–4357.
14 W. T. Hong, M. Risch, K. A. Stoerzinger, A. Grimaud, J. Suntivich and Y. Shao-Horn, *Energy Environ. Sci.*, 2015, **8**, 1404–1427.
15 R. D. L. Smith, M. S. Prevot, R. D. Fagan, S. Trudel and C. P. Berlinguette, *J. Am. Chem. Soc.*, 2013, **135**, 11580–11586.
16 M. Gong, Y. Li, H. Wang, Y. Liang, J. Z. Wu, J. Zhou, J. Wang, T. Regier, F. Wei and H. Dai, *J. Am. Chem. Soc.*, 2013, **135**, 8452–8455.
17 M. W. Louie and A. T. Bell, *J. Am. Chem. Soc.*, 2013, **135**, 12329–12337.
18 L. Trotochaud, S. L. Young, J. K. Ranney and S. W. Boettcher, *J. Am. Chem. Soc.*, 2014, **136**, 6744–6753.
19 D. A. Corrigan, *J. Electrochem. Soc.*, 1987, **134**, 377–384.
20 M. Görlin, P. Chernev, J. Ferreira de Araújo, T. Reier, S. Dresp, B. Paul, R. Krähnert, H. Dau and P. Strasser, *J. Am. Chem. Soc.*, 2016, **138**, 5603–5614.
21 S. Dresp, F. Dionigi, S. Loos, J. Ferreira de Araujo, C. Spöri, M. Gliech, H. Dau and P. Strasser, *Adv. Energy Mater.*, 2018, **8**, 1800338.
22 R. D. L. Smith, C. Pasquini, S. Loos, P. Chernev, K. Klingan, P. Kubella, M. R. Mohammadi, D. González-Flores and H. Dau, *Energy Environ. Sci.*, 2018, **11**, 2476–2485.
23 D. González-Flores, K. Klingan, P. Chernev, S. Loos, M. R. Mohammadi, C. Pasquini, P. Kubella, I. Zaharieva, R. D. L. Smith and H. Dau, *Sustainable Energy Fuels*, 2018, **2**, 1986–1994.
24 M. K. Bates, Q. Jia, H. Doan, W. Liang and S. Mukerjee, *ACS Catal.*, 2016, **6**, 155–161.
25 H. Xiao, H. Shin and W. A. Goddard, *Proc. Natl. Acad. Sci. U. S. A.*, 2018, **115**, 5872–5877.
26 N. Li, D. K. Bediako, R. G. Hadt, D. Hayes, T. J. Kempa, F. von Cube, D. C. Bell, L. X. Chen and D. G. Nocera, *Proc. Natl. Acad. Sci. U. S. A.*, 2017, **114**, 1486.
27 D. Friebel, M. W. Louie, M. Bajdich, K. E. Sanwald, Y. Cai, A. M. Wise, M.-J. Cheng, D. Sokaras, T.-C. Weng, R. Alonso-Mori, R. C. Davis, J. R. Bargar, J. K. Nørskov, A. Nilsson and A. T. Bell, *J. Am. Chem. Soc.*, 2015, **137**, 1305–1313.
28 D. Wang, J. Zhou, Y. Hu, J. Yang, N. Han, Y. Li and T.-K. Sham, *J. Phys. Chem. C*, 2015, **119**, 19573–19583.
29 Z. K. Goldsmith, A. K. Harshan, J. B. Gerken, M. Voros, G. Galli, S. S. Stahl and S. Hammes-Schiffer, *Proc. Natl. Acad. Sci. U. S. A.*, 2017, **114**, 3050–3055.
30 J. Y. C. Chen, L. Dang, H. Liang, W. Bi, J. B. Gerken, S. Jin, E. E. Alp and S. S. Stahl, *J. Am. Chem. Soc.*, 2015, **137**, 15090–15093.
31 B. M. Hunter, N. B. Thompson, A. M. Müller, G. R. Rossman, M. G. Hill, J. R. Winkler and H. B. Gray, *Joule*, 2018, **2**, 747–763.
32 H. S. Ahn and A. J. Bard, *J. Am. Chem. Soc.*, 2016, **138**, 313–318.
33 M. Burke Stevens, C. D. M. Trang, L. J. Enman, J. Deng and S. W. Boettcher, *J. Am. Chem. Soc.*, 2017, **139**, 11361–11364.
34 H. Yin, L. Jiang, P. Liu, M. Al-Mamun, Y. Wang, Y. L. Zhong, H. Yang, D. Wang, Z. Tang and H. Zhao, *Nano Res.*, 2018, **11**, 3959–3971.
35 J. Wang, L. Gan, W. Zhang, Y. Peng, H. Yu, Q. Yan, X. Xia and X. Wang, *Sci. Adv.*, 2018, **4**, eaap7970.
36 D. S. Hall, D. J. Lockwood, C. Bock and B. R. MacDougall, *Proc. R. Soc. London, Ser. A*, 2015, **471**, 1–65.
37 M. P. Browne, S. Stafford, M. O'Brien, H. Nolan, N. C. Berner, G. S. Duesberg, P. E. Colavita and M. E. G. Lyons, *J. Phys. Chem. A*, 2016, **4**, 11397–11407.
38 F. Dionigi and P. Strasser, *Adv. Energy Mater.*, 2016, **6**, 1600621.
39 J. D. Michael, E. L. Demeter, S. M. Illes, Q. Fan, J. R. Boes and J. R. Kitchin, *J. Phys. Chem. C*, 2015, **119**, 11475–11481.
40 S. Klaus, M. W. Louie, L. Trotochaud and A. T. Bell, *J. Phys. Chem. C*, 2015, **119**, 18303–18316.
41 F. D. Speck, K. E. Dettelbach, R. S. Sherbo, D. A. Salvatore, A. Huang and C. P. Berlinguette, *Chem*, 2017, **2**, 590–597.